Journal of Atmospheric and Solar-Terrestrial Physics 119 (2014) 83–90

Contents lists available at ScienceDirect

Journal of Atmospheric and Solar-Terrestrial Physics

journal homepage: www.elsevier.com/locate/jastp

Stratospheric and mesospheric concentric gravity waves over tropical cyclone Mahasen: Joint AIRS and VIIRS satellite observations

Jia Yue [a,*], Steven D. Miller [b], Lars Hoffmann [c], William C. Straka III [d]

[a] Atmospheric and Planetary Sciences, Hampton University, VA, USA
[b] Cooperative Institute for Research in the Atmosphere, Colorado State University, Fort Collins, CO, USA
[c] Jülich Supercomputing Centre, Forschungszentrum Jülich, Jülich, Germany
[d] Cooperative Institute for Meteorological Satellite Studies, University of Wisconsin Madison, Madison, WI, USA

ARTICLE INFO

Article history:
Received 14 May 2014
Received in revised form
8 July 2014
Accepted 9 July 2014
Available online 16 July 2014

Keywords:
T
S

ABSTRACT

We report on the first simultaneous spaceborne observations of concentric gravity wave patterns in the stratosphere and mesosphere over the Indian Ocean excited by Tropical Cyclone Mahasen. On the nights of 13–14 May 2013, concentric ring patterns in nightglow were observed in close-proximity to Mahasen by the Day/Night Band (DNB) of the Visible/Infrared Imager/Radiometer Suite (VIIRS) on the Suomi NPP satellite. The waves exhibited horizontal wavelengths of 40–60 km. On 13 May 2013, long concentric waves of ~500 km wavelength were also seen west of India, far away (~1500 km) from their estimated center near Mahasen. Concentric gravity waves in the stratosphere were observed nearly simultaneously by the Atmospheric Infrared Sounder on the Aqua satellite. These multi-level observations provide a clearer picture of the complex three-dimensional structure of tropical cyclone-generated gravity waves than a single instrument alone.

1. Introduction

Tropical cyclones (TCs) are classified according to their maximum sustained winds and the oceanic basin they are located in Neumann (1993). The weakest systems are generally classified as tropical depressions and tropical storms, while the strongest are labeled as Hurricanes (in the western North Atlantic and eastern North Pacific), Typhoons (western North Pacific Ocean), Cyclonic Storms (Indian Ocean), or simply Tropical Cyclones (Australia/South Pacific). Generally, intense TCs are a significant source of gravity waves (hereafter, TC-generated gravity waves, or TGW) that propagate through the upper troposphere, stratosphere, and mesosphere (Pfister et al., 1993; Sato, 1993; Chane-Ming et al., 2002; Dhaka et al., 2003; Kim et al., 2009). The horizontal wavelengths of TGWs are typically in the range of 50–500 km, with periods from 1 h to 1.6 days (Kim et al., 2009). For an example of a TGW in the mesosphere, Suzuki et al. (2013) reported fragments of concentric rings of TGWs observed by a chain of OH airglow imaging systems over Japan. To investigate the propagation of TGWs from the troposphere to the mesosphere, several field experiments have been carried out in Australia, for example, the Tropical Warm Pool International Cloud Experiment (TWP-ICE) (Evan and Alexander, 2008; Hecht et al., 2009) and the Darwin Area Wave Experiment (DAWEX) (Hamilton et al., 2004). In particular, Hecht et al. (2009) showed that some TGWs were likely ducted in a trapped region, i.e., the mesospheric inversion layer.

Mesoscale numerical models, such as the three-dimensional mesoscale model (MM5) and Weather Research Forecasting (WRF) model, have been used to study the characteristics of TGWs, including their influence on the background flow and on the TCs themselves (Kim et al., 2005, 2009; Kuester et al., 2008; Kim and Chun, 2010, 2011). However, these mesoscale models usually extend only to the stratosphere (~30 km for MM5 and ~45 km for standard WRF) (Dudhia, 1993; Skamarock et al., 2005). Therefore, TGWs in airglow cannot be easily simulated in these models. Kuester et al. (2008) suggest that the obstacle effect mechanism generates most of the TGWs with the phase speed being equal to the speed of the moving heat source, while the deep heating mechanism contributes to TGWs with high phase speed.

Compared to terrestrial-based (e.g., surface and aircraft) observational data, Earth-viewing polar-orbiting satellite instruments hold the advantage of global coverage to observe TGWs on a horizontal plane (Kim et al., 2009). This vantage point provides an ability to resolve the full extent of wave patterns which may span hundreds or even thousands of km. Unlike ground-based optical measurements, spaceborne observations of TGWs are not prohibited by clouds and poor weather (Yue et al., 2013). On the other hand, the resolution of most of the Earth

* Corresponding author.
E-mail address: jia.yue@hamptonu.edu (J. Yue).

http://dx.doi.org/10.1016/j.jastp.2014.07.003
1364-6826/

viewing satellites is much coarser than ground-based imaging systems. Therefore, they are not sensitive to small-scale GWs. Only AIRS and VIIRS observations do not provide altitude-dependent information about GWs. Sensors on polar-orbiting satellites only pass the same place twice a day. Thus, the temporal evolution of GWs cannot be observed and wave phase speed and period cannot be measured.

In this paper, we report on a TGW event that occurred over 13–14 May 2013. The event was associated with the first named storm of the 2013 season in the Bay of Bengal, TC Mahasen. The TC was later renamed Cyclonic Storm Viyaru by the Regional Specialized Meteorology Center (RSMC) New Delhi, India Meteorological Department. The system produced a complete concentric TGW pattern, visible in the nightglow from a new spaceborne instrument, the Visible/Infrared Imager/Radiometer Suite Day/Night Band (VIIRS/DNB, which is carried on board the Suomi National Polar-orbiting Partnership (NPP) satellite, described in more detail below). Because the Suomi NPP and the National Aeronautics and Space Administration (NASA) Aqua satellites fly in the same orbital plane, we are able to report joint observations from two satellites when their orbits were in-phase. On one of the nights, as Mahasen was gathering strength in the Bay of Bengal, both stratospheric and mesospheric TGWs were observed nearly simultaneously by Suomi NPP and Aqua, providing an unprecedented perspective on this complex TGW event.

2. Data sets

2.1. AIRS observations

The Atmospheric Infrared Sounder (AIRS) onboard the NASA Aqua satellite is a grating spectrometer measuring the thermal emission of atmospheric constituents in the nadir through sub-limb viewing geometry (Aumann et al., 2003). Aqua is in a Sun-synchronous polar orbit (13:30 local time, ascending node) at 705 km altitude and 99 min period. AIRS radiance measurements at the 4.3 μm CO_2 fundamental band are used to detect TGW-induced temperature perturbations between 30 and 40 km above mean sea level (AMSL) (Hoffmann et al., 2013). The AIRS radiance measurements at 8.1 μm (an atmospheric window channel) are used to detect the presence of convection and anvil clouds associated with tropical cyclones (Aumann et al., 2006; Hoffmann et al., 2013; Yue et al., 2013). The footprint size of AIRS is 13–14 km diameter at nadir view and 41 km × 21.4 km at the scan edges. The swath width is 1765 km, which is sufficient to cover the horizontal scale of most tropical storm systems.

2.2. VIIRS day night band observations

VIIRS is a scanning optical sensor with very high spatial resolution (nadir values of 0.375 km for imagery resolution bands, 0.75 km for moderate resolution bands) and a 3000 km across-track swath width. VIIRS is one of the six instruments flying on the NASA Suomi NPP satellite launched on 28 October 2011. NPP flies in a Sun-synchronous orbit at ~834 km altitude. Both Aqua and NPP have local equatorial crossing times of ~1:30 p.m. (ascending node) and 1:30 a.m. (descending node), and since Aqua's orbital altitude is slightly lower (705 km), it 'laps' Suomi every 2–3 days.

VIIRS includes a next-generation low-light sensor, the DNB. The DNB is a broadband passive radiometer with a spectral response of 505–890 nm. The DNB provides extremely high sensitivity to low-light signals via three levels of gain amplification—achieving detection down to levels of $\sim 10^{-5}$ W m^{-2} sr^{-1}, or roughly 10^6 times more sensitive than most conventional visible-band sensors. The spectral response happens to overlap with the dominant OH Meinel bands in the near infrared (NIR). The sensor has demonstrated the ability to sense a wide array of nocturnal phenomena, both natural and anthropogenic, via observations of terrestrial emissions and lunar reflection (Miller et al., 2013). In addition to the anticipated capabilities, Miller et al. (2012) describe the DNB's unexpected sensitivity to both reflected and direct-emission nightglow. Particularly germane to the current study, Miller et al. (2012) show an example of a DNB-observed GW event in the nightglow above a thunderstorm in the tropical Pacific Ocean.

While the forcing of GWs by tropospheric phenomenon such as convection and topography all well known, the Miller et al. (2012) study documents the first mesospheric GWs in nightglow to be observed at sub-km resolution by a nadir-viewing instrument from space. The horizontal wavelength of ~33 km and concentric ring structures of the observed waves were consistent with convectively generated gravity waves previously observed by ground-based airglow imagers (e.g., Taylor and Haphood, 1988; Sentman et al., 2003; Suzuki et al., 2007; Vadas et al., 2012; Yue et al., 2009, 2013). With its high sensitivity, high spatial resolution, and wide swath the DNB is capable of observing both small-scale and large-scale TGWs. One limitation of the DNB is its coarse temporal resolution – offering only 1 pass per night at lower latitudes and thus unable to provide information on the phase speeds as well as propagation direction of the various wave

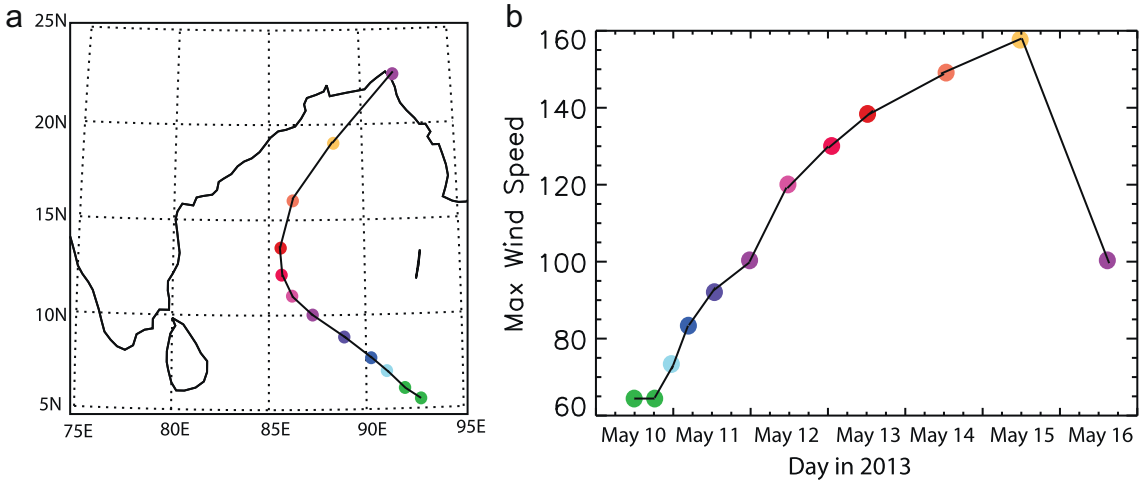

Fig. 1. (a) Trajectory and (b) maximum wind speed (km/h) of TC Mahasen during 10–16 May 2013 (from Global Disaster Alert and Coordination System http://www.gdacs.org/Cyclones/report.aspx?episodeid=6&eventid=37639&eventtype=TC).

structures. Another limitation is its sub-optimal band-pass for nightglow observations, and the fact that the very faint signals reside just above the noise floor of the sensor—making for grainy imagery and ambiguity between directly-emitted nightglow GW signals and contamination signals such as clouds reflecting the downwelling nightglow.

3. Results

3.1. Tropical cyclone Mahasen

TC Mahasen formed from a low pressure in the southern Bay of Bengal in early May 2013. On 10 May 2013 Mahasen strengthened into a tropical depression. The system was classified by RSMC New Delhi as a named storm on 11 May 2013, when it attained gale-force surface winds (17.5–24.2 m/s). Fig. 1 displays a trace of TC Mahasen's track and its maximum wind speed. The storm evolved into a tropical cyclone moving northwestward on 11 May 2013. On 14 May, Mahasen turned toward the northeast and on 16 May 2013 it reached peak intensity with a central pressure of 990 hPa. Shortly thereafter, Mahasen made landfall in Bangladesh and had dissipated by 17 May 2013 near Mizoram, India. In the context of the full 2013 North Indian Ocean cyclone season, Mahasen was a relatively weak TC. However, strong latent heat release by convective bursts during portions of the storm's intensification phase was sufficient to produce a remarkable display of TGWs which are the focus of the current study.

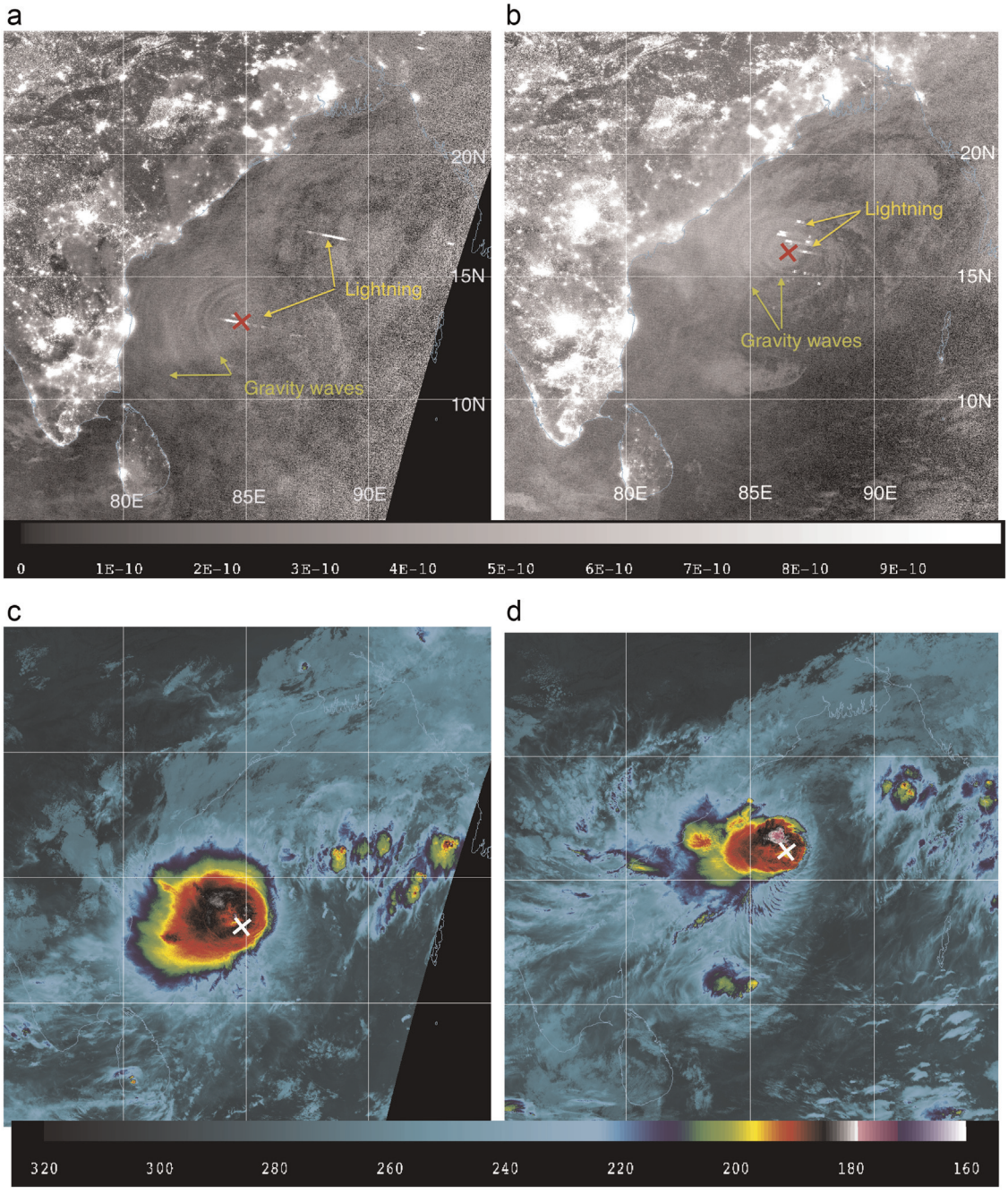

Fig. 2. DNB observations ($\log_{10}$-scaled in W cm^2 sr^{-1}) of the TGWs on (a) 13 May and (b) 14 May, 2013; and corresponding infrared window (brightness temperature in K) observations of TC Mahasen in (c) and (d). Red and white crosses denote the estimated centers of the concentric TGW structures. (For interpretation of the references to color in this figure legend, the reader is referred to the web version of this article.)

3.2. DNB observations

Fig. 2 displays the DNB and infrared 10.76 μm band observations of Mahasen's TGWs on 13 and 14 May 2013. During this period, the moon was in the early waxing crescent phase of the lunar cycle, and was thus well below the horizon at the time of the NPP overpass. As reported by Miller et al. (2012), all cloud structures and the TGWs themselves are the result of nightglow reflection and direct emission, respectively. Owing to the inherent sensitivity of the DNB, anthropogenic light sources, in particular the lights from cities in India and Sri Lanka are clearly visible in the DNB, along with a few lights from maritime vessels in Bay of Bengal. The brightest land-based anthropogenic light sources represent large metropolitan areas like Chennai, Hyderabad, and Bangalore. On the night of 13 May 2013, a group of concentric GW rings emanating from the storm (denoted by the green arrows in Fig. 2a) were observed over the Indian Ocean in the region of (10–17° N, 80–85° E). These waves had variable horizontal wavelengths in their inner and outer rings. The inner rings are most clear and their horizontal wavelength is measured to be ~60 km. To determine the center of these concentric GWs, we fit circles of varying radii and centers to each ring, and look for optimal matches (Yue et al., 2009; Suzuki et al., 2013). The center of the rings was located near (13° N, 85° E; denoted by the red cross). Without continuous observations over this region, the periods and propagating velocities of these waves cannot be measured (Yue et al., 2013). A geostationary low-light sensor of similar sensitivity to the DNB, or further optimized to sensing the nightglow emissions, could supply such information in the future. The DNB also observed several lightning strikes in the vicinity of the TC core (noted in Fig. 2a). These manifest in DNB imagery as along-scan bright segments (~12 km wide strips formed by 16 adjacent simultaneously observed scan lines), with variable horizontal extent depending on flash duration and the degree of light diffusion (multiple scatter within the cloud). Simultaneous thermal infrared cloud observations of TC Mahasen are shown in Fig. 2c and d. The TGW ring patterns are not evident in the thermal imagery, and in some areas the rings are seen to extend well beyond the horizontal boundaries of the underlying meteorological clouds, confirming that these structures are indeed tied to the nightglow emission. The white cross (same as the red cross in Fig. 2a), indicating the location of the wave centers, is near the center of Mahasen. Because these TGWs are relatively small-scale, it is plausible that they were excited by strong latent heat release or overshooting occurring within the deep convection of the TC system (Kuester et al., 2008; Yue et al., 2009).

Interestingly, besides the small-scale TGWs (~60 km horizontal wavelength), large-scale concentric GWs were also seen west of India on 13 May 2013, denoted by blue arrows in Fig. 3. The center of these GWs, estimated by the same technique as described above, was determined to be also near TC Mahasen, suggesting that they were tied to Mahasen ~1500 km away as well. These GWs displayed horizontal wavelengths of about 500 km, similar to the scale of Mahasen itself, as shown in Fig. 2c. Considering the TC as a "moving mountain", such large-scale TGWs could have been excited via the obstacle mechanism (Kuester et al., 2008). Yue et al. (2013) report on similar large-scale GWs observed by AIRS, which were excited by a large storm system in continental North America. Note here that only a few apparent monochromatic waves are observed in Fig. 3 instead of a broad spectrum near the source. This can be due to the different propagation times from the troposphere to the mesosphere. Waves with different wavelengths would need different times, even if they are launched at the same point.

Similar TGW structures were observed on the following night of 14 May 2013 (Fig. 2b) when Mahasen moved northeastward (Fig. 2d), although the longer-wavelength TGWs in the Arabian Sea were not observed. While the horizontal extent of Mahasen contracted over the period, the center of the storm became colder as it gained strength. The TGWs were again observed to emanate westward and northwestward with a horizontal wavelength of ~40 km. The estimated center of these TGWs is located the southeast of the storm center at roughly (16° N, 87° E). Again, the DNB observed several lightning strikes observed in the core of the storm, consistent with the presence of strong convection which could account for the TGW generation. The presence of TGWs in two consecutive nights demonstrates the prolific nature of TCs as a source for these GWs. With its broad spatial coverage, high sensitivity, high spatial resolution, and multi-spectral information, VIIRS offers the first complete depiction of concentric TGW patterns manifested in nightglow, coupled with simultaneous observations of the clouds of the parent TC.

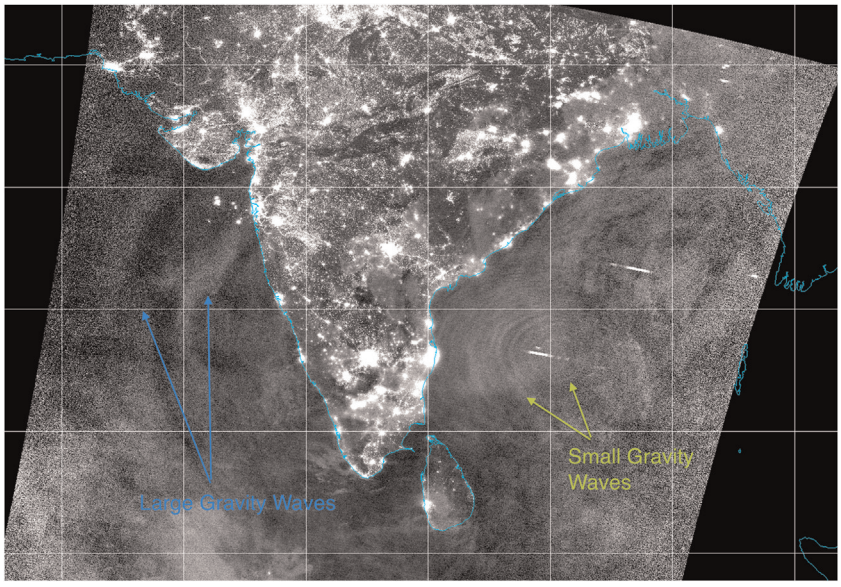

Fig. 3. Zoom-out image of DNB observation of concentric TGWs on 13 May 2013. Short-wavelength TGWs near storm center are denoted by green arrows, while longer wavelength TGWs to the west of India are denoted by blue arrows. (For interpretation of the references to color in this figure legend, the reader is referred to the web version of this article.)

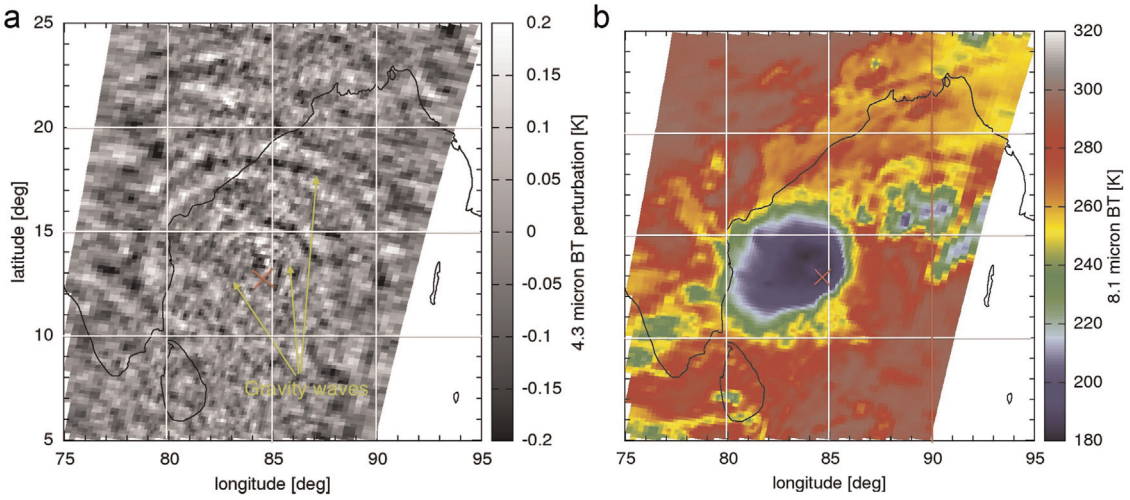

Fig. 4. AIRS observations of (a) stratospheric TGWs in 4.3 μm radiance and (b) cloud observations in 8.1 μm radiance of TC Mahasen on 13 May 2013 around 2010 UT. The red cross denotes the estimated center of concentric GWs. (For interpretation of the references to color in this figure legend, the reader is referred to the web version of this article.)

3.3. AIRS observations

Fig. 4 displays the AIRS observations of TGWs and clouds of TC Mahasen on 13 May 2013. As mentioned previously, Aqua and Suomi NPP share a common orbital plane and therefore have the same local equatorial crossing times. However, owing to their different orbit altitudes they do not share identical ground tracks, and the two satellites are only perfectly overlapped in space and time for a brief span of several hours every 2–3 days. Fortunately, the two satellites were nearly in-phase at the time of the 13 May Mahasen overpass. In particular, between 1445 UTC and 1919 UTC, the two satellites were within 3.5 min (~1500 km) of each other. For the purposes of this comparison and considering the time scales of GW propagation, the AIRS and DNB observations may be regarded as nearly simultaneous. The horizontal resolution of AIRS is much lower compared to the DNB; thus it cannot resolve fine structures. Note also that the AIRS TGW observations are noise limited, with the stratospheric wave amplitudes being a factor of ~40 smaller than the mesospheric wave amplitudes (Yue et al., 2013). Nevertheless, the TGW signatures of TC Mahasen are still readily identified in the AIRS data.

The stratospheric TGWs in the 4.3 μm radiance perturbations (with sensitivity near 30–40 km AMSL) were observed to be propagating eastward, northward, and westward. Both small-scale TGWs in the region of (13–15° N, 82–85° E), and medium-scale TGWs around (15–20° N, 80–90° E) were noted. The former exhibited horizontal wavelengths of ~60 km, while the latter had wavelengths of ~150 km. The centers of these waves (denoted by the red cross in Fig. 4) were found to be very close to the center of the TGWs in the DNB observations (red crosses in Fig. 2). This suggests that the TGWs in AIRS and DNB were likely excited by a common source. The large-scale TGWs in Fig. 3 are not seen in AIRS. On 14 May 2013, Mahasen and its associated TGWs resided in a coverage gap between two adjacent AIRS swaths, therefore, no AIRS observations were available. However, medium-scale TGWs were observed by AIRS on other days (not shown) throughout the life-cycle of Mahasen.

3.4. AIRS and DNB comparison

Comparing Figs. 2a and 4a, the small-scale TGWs with a horizontal wavelength of ~60 km in the stratosphere and

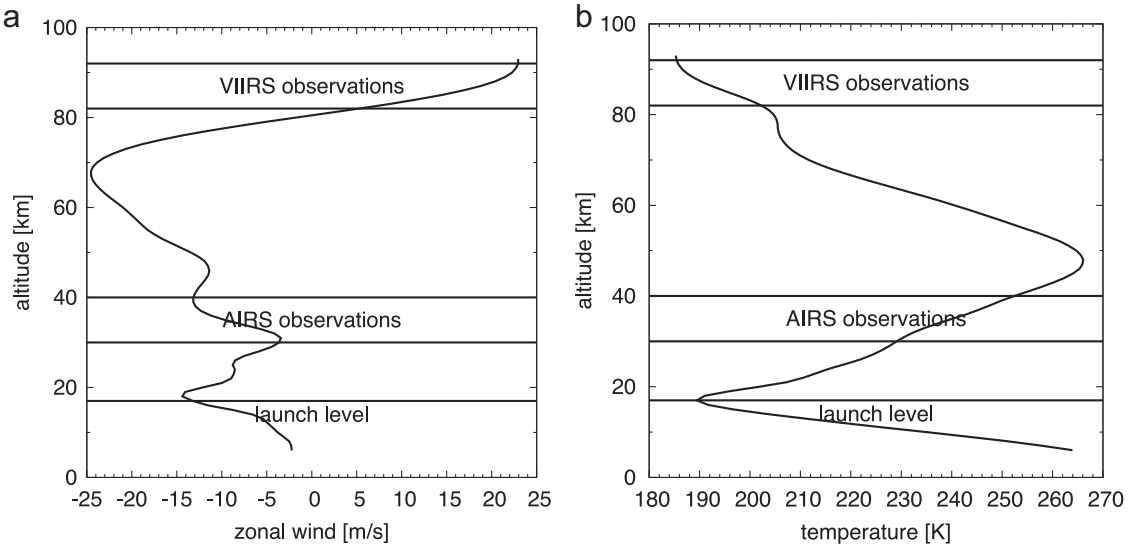

Fig. 5. Profiles of (a) zonal wind and (b) temperature. The profiles are composed of ERA-Interim data below 50 km and TIME-GCM data above 50 km.

mesosphere are approximately collocated in (83–85° E, 12–15° N). The AIRS-observed TGWs in Fig. 4 were mainly propagating eastward, northward, and westward, while the DNB TGWs in Fig. 2 were found to be heading only westward and northward. Several factors may account for the absence of TGWs propagating eastward in nightglow. The background wind field between the mid-stratosphere (30–40 km) and the mesopause (85 km) can effectively filter out parts of the GWs. The filtering occurs when the phase velocity of the TGWs is equal to the wind velocity in the direction of propagation. Fig. 5a displays the resembled background wind from ERA-Interim and climatology from the Thermosphere-Ionosphere-Mesosphere-Electrodynamics General Circulation Model (TIME-GCM) (Yue et al., 2013, 2014). The maximum background zonal wind between the stratosphere and the mesopause on 13 May 2013 is −25 m/s (westward). This cannot filter out eastward propagating TGWs.

The wind in the stratosphere and mesosphere can alter the vertical wavelength of TGWs. AIRS can only detect stratospheric GWs having vertical wavelengths longer than ~20 km, while the DNB can only see mesospheric GWs having vertical wavelengths longer than ~10 km (Yue et al., 2013). To estimate the TGW propagation from the tropospheric source through the stratosphere towards the airglow layer (~90 km), we conducted ray tracing simulations using the background temperature and wind profiles in Fig. 5 (Alexander, 1996; Yue et al., 2013, 2014). GWs with two vertical wavelengths of 17 km and 34 km (representing 1× to 2× the depth of the tropopause) and three horizontal wavelengths (60 km, 150 km, and 500 km) were calculated. Fig. 6 shows the calculated vertical wavelengths. Because of the eastward wind at the mesopause (Fig. 5a), the vertical wavelengths of eastward propagating TGWs are substantially reduced near the airglow layer, while the vertical wavelengths of westward TGWs are enlarged. This facilitates the observation of westward TGWs in the airglow, especially for the small-scale GWs.

We also calculated the travel distance and time for the westward-propagating TGWs using the ray tracing simulation, as shown in Fig. 7. The model shows that the large-scale TGW of ~500 km horizontal wavelength traveled a distance of 1000–2000 km distance (consistent with Fig. 3) and 2–7 h from the source to the airglow layer. The northward or westward-propagating small-scale TGWs with 60 km horizontal wavelength (in Figs. 2a and 4a) travel ~50 km horizontally and ~10–20 min from the stratosphere to the mesopause. Therefore, these TGWs in VIIRS and AIRS were collocated in nearly simultaneous observations. The ray tracing simulations provide further evidence that the TGWs by both AIRS and VIIRS originate from the same source.

For freely propagating TGWs and weak background wind, the period of the wave can be estimated from

$$cos(\alpha) = \omega/N \quad (1)$$

where α is defined as the angle between the wave vector and the zenith, ω is the wave frequency, and N is the Boussinesq frequency (approximately $2\pi/5\ \mathrm{min}^{-1}$ at the mesopause). The elevation angle can be calculated from the OH layer altitude (~87 km) minus the source level (~20 km), and the horizontal distance to the source. Using Eq. (1), we can estimate that the period for the large-scale TGWs (1500 km away from the source) in Fig. 3 is ~110 min. With a horizontal wavelength of ~500 km, the phase speed is ~75 m/s. It takes ~5 h to travel. This is consistent with the ray trace calculation.

4. Summary

This paper reports the first simultaneous space-borne observations of TGWs in the stratosphere and mesosphere, enabled by the unique pairing of AIRS on Aqua and the new VIIRS/DNB on Suomi NPP, respectively. Even though AIRS-observed TGWs have been documented previously (Kim et al., 2009), this study captures the first coupling of such observations with TGW observations near the mesopause via nightglow. There is a growing compilation of DNB-observed TGWs (including Supertyphoon Haiyan in November 2013); a more in-depth study of these TGW events by the DNB and other instruments is planned.

Both small-scale (40–60 km wavelength) and large-scale (~500 km wavelength) concentric TGWs were observed from VIIRS in the nightglow structures for the same time and for the first time. The small waves could be excited locally by deep

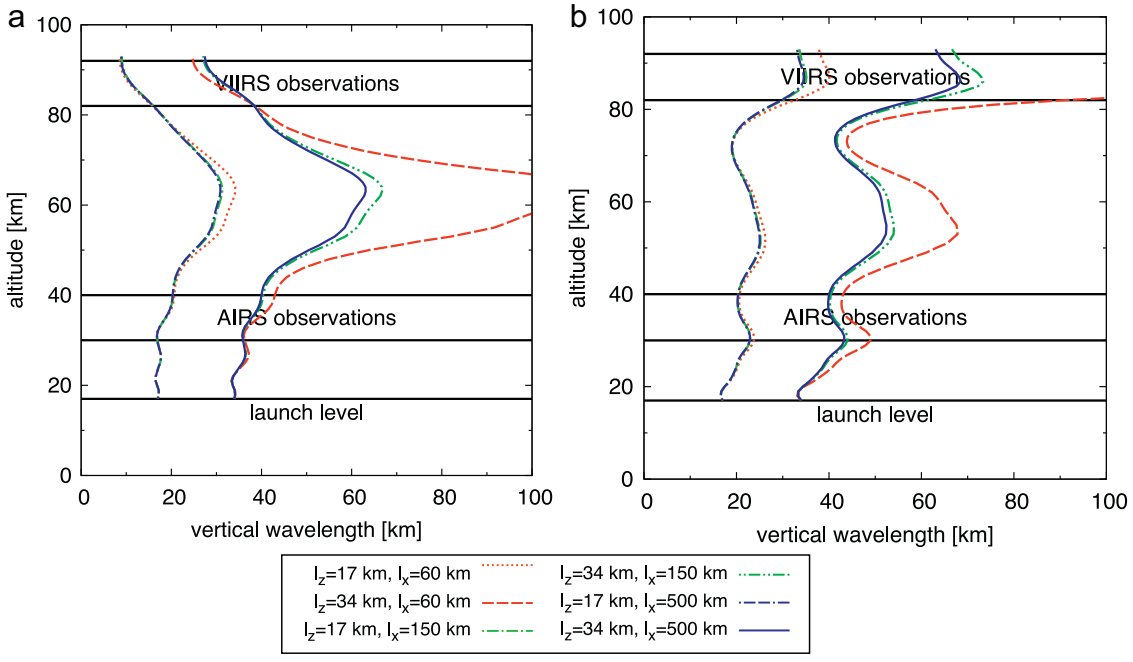

Fig. 6. Evolution of vertical wavelengths for (a) eastward propagating TGWs and (b) westward propagating TGWs. Different horizontal and vertical wavelengths at the source are denoted by different colors and line styles. (For interpretation of the references to color in this figure legend, the reader is referred to the web version of this article.)

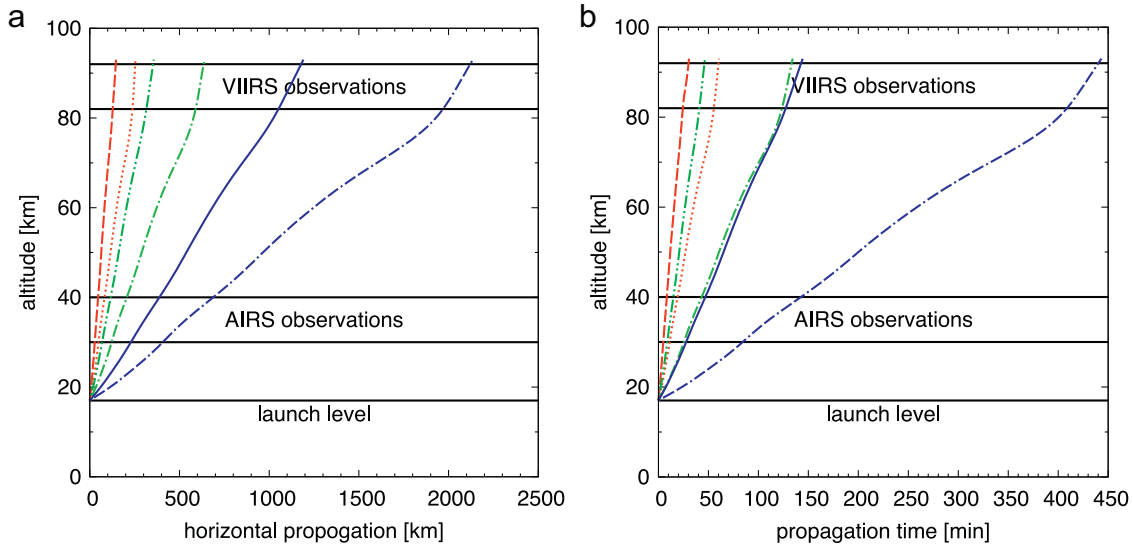

Fig. 7. (a) Propagation distance and (b) propagation time from the source at 20 km for the six TGWs. The definition of line colors and line styles are the same as Fig. 6. (For interpretation of the references to color in this figure legend, the reader is referred to the web version of this article.)

latent-heating mechanisms or overshooting within the TC eyewall and spiral rainbands, and the larger remote ones could be launched via the obstacle effect, as suggested by Kuester et al. (2008). These satellite observations provide direct validation for future mesoscale cloud-resolving model simulations of TGWs. Combining DNB and AIRS observations with other measurements from the DAWEX or TWP-ICE campaigns (e.g., Hecht et al., 2009), future field experiments will yield more detailed information about TGWs.

Acknowledgment

AIRS data are distributed by the NASA Goddard Earth Sciences Data Information and Services Center (DISC). The VIIRS Sensor Data Record data are distributed by the CIMSS Atmospheric Product and Evaluation and Test Elements (PEATE) and NOAA Comprehensive Large Array-data Stewardship System (CLASS). JY is supported by the NASA AIM Mission and NASA Heliophysics Supporting Research Grant NNX14AF20G. SDM acknowledges support of the NOAA Joint Polar Satellite System Cal/Val and Algorithm Program and the Naval Research Laboratory (BAA Grant #N00173-14-1-G902). We are grateful to Joan Alexander for access to a ray tracing code. We thank the reviewer for his/her helpful comments.

References

Alexander, M.J., 1996. A simulated spectrum of convectively generated gravity waves: Propagation from the tropopause to the mesopause and effects on the middle atmosphere. J. Geophys. Res. 101 (D1), 1571–1588, http://dx.doi.org/10.1029/95JD02046.

Aumann, H.H., et al., 2003. AIRS/AMSU/HSB on the Aqua mission: design, science objective, data products, and processing systems. IEEE Trans. Geosci. Remote Sens 41, 253–264.

Aumann, H.H., Gregorich, D., DeSouza-Machado, S.M., 2006. AIRS observations of deep convective clouds. Proc. SPIE 6301, 63010J, http://dx.doi.org/10.1117/12.681201.

Chane-Ming, F., Roff, G., Robert, L., Leveau, J., 2002. Gravity wave characteristics over Tromelin Island during the passage of cyclone Hudah. Geophys. Res. Lett. 29 (6), 1094, http://dx.doi.org/10.1029/2001GL013286.

Dhaka, S.K., Takahashi, M., Shibagaki, Y., Yamanaka, M.D., Fukao, S., 2003. Gravity wave generation in the lower stratosphere due to passage of the typhoon 9426 (Orchid) observed by the MU radar at Shigaraki (34.85°N, 136.10°E). J. Geophys. Res. 108 (D19), 4595, http://dx.doi.org/10.1029/2003JD003489.

Dudhia, J., 1993. A nonhydrostatic version of the Penn State–NCAR mesoscale model: Validation tests and simulation of an Atlantic cyclone and cold front. Mon. Weather Rev. 121, 1493–1513.

Evan, S., Alexander, M.J., 2008. Intermediate-scale tropical inertia gravity waves observed during the TWP-ICE campaign. J. Geophys. Res. 113, D14104, http://dx.doi.org/10.1029/2007JD009289.

Hamilton, K., Vincent, R.A., May, P.T., 2004. Darwin Area Wave Experiment (DAWEX) field campaign to study gravity wave generation and propagation. J. Geophys. Res. 109, D20S01, http://dx.doi.org/10.1029/2003JD004393.

Hecht, J.H., et al., 2009. Imaging of atmospheric gravity waves in the stratosphere and upper mesosphere using satellite and ground-based observations over Australia during the TWPICE campaign. J. Geophys. Res. 114, D18123, http://dx.doi.org/10.1029/2008JD011259.

Hoffmann, L., Xue, X., Alexander, M.J., 2013. A global view of stratospheric gravity wave hotspots located with Atmospheric Infrared Sounder observations. J. Geophys. Res. Atmos. 118, 416–434, http://dx.doi.org/10.1029/2012JD018658.

Kim, S.-Y., Chun, H.-Y., Baik, J.-J., 2005. A numerical study of gravity waves induced by convection associated with Typhoon Rusa. Geophys. Res. Lett. 32, L24816, http://dx.doi.org/10.1029/2005GL024662.

Kim, S.-Y., Chun, H.-Y., Wu, D.L., 2009. A study on stratospheric gravity waves generated by Typhoon Ewiniar: numerical simulations and satellite observations. J. Geophys. Res. 114, D22104, http://dx.doi.org/10.1029/2009JD011971.

Kim, S.-Y., Chun, H.-Y., 2010. Stratospheric gravity waves generated by Typhoon Saomai (2006): numerical modeling in a moving frame following the typhoon. J. Atmos. Sci. 67, 3617–3636, http://dx.doi.org/10.1175/2010JAS3374.1.

Kim, S.-Y., Chun, H.-Y., 2011. Impact of typhoon-generated gravity waves in the typhoon development. Geophys. Res. Lett. 38, L01806, http://dx.doi.org/10.1029/2010GL045719.

Kuester, M.A., Alexander, M.J., Ray, E.A., 2008. A model study of gravity waves over Hurricane Humberto (2001). J. Atmos. Sci. 65, 3231–3246, http://dx.doi.org/10.1175/2008JAS2372.1.

Miller, S.D., Mills, S.P., Elvidge, C.D., Lindsey, D.T., Lee, T.F., Hawkins, J.D., 2012. Suomi satellite brings to light a unique frontier of nighttime environmental sensing capabilities. Proc. Natl. Acad. Sci. U. S. A. 109, 39, http://dx.doi.org/10.1073/pnas.1207034109.

Miller, S.D., Straka III, W., Mills, S.P., Elvidge, C.D., Lee, T.F., Solbrig, J., Walther, A., Heidinger, A.K., Weiss, S.C., 2013. Illuminating the capabilities of the Suomi NPP VIIRS Day/Night Band. Remote Sens. 5, 6717–6766, http://dx.doi.org/10.3390/rs5126717.

Neumann, C.J., 1993. Global overview: Global Guide to Tropical Cyclone Forecasting,. World Meteorological Organization, Geneva, Switzerland. (WMO/TC-No. 560, Report No. TCP-31).

Pfister, L., Chan, K.R., Bui, T.P., Bowen, S., Legg, M., Gary, B., Kelly, K., Proffitt, M., Starr, W., 1993. Gravity waves generated by a tropical cyclone during the STEP tropical field program: a case study. J. Geophys. Res. 98, 8611–8638, http://dx.doi.org/10.1029/92JD01679.

Sato, K., 1993. Small-scale wind disturbances observed by the MU radar during the passage of Typhoon Kelly. J. Atmos. Sci. 50, 518–537. (doi:10.1175/1520-0469(1993)050 < 0518:SSWDOB > 2.0.CO;2.).

Sentman, D.D., Wescott, E.M., Picard, R.H., Stenbaek-Nielsen, H.C., Dewan, E.M., Moudry, D.R., Sao Sabbas, F.T., Heavner, M.J., Morrill, J., 2003. Simultaneous observations of mesospheric gravity waves and sprites generated by a mid-westerm thunderstorm. J. Atmos. Terr. Phys. 65, 537–550, http://dx.doi.org/10.1016/S1364-6826(02)00328-0.

Skamarock, W.C., J.B. Klemp, J. Dudhia, D.O. Gill, D.M. Barker, W. Wang, and J.G. Power (2005), A description of the Advanced Research WRF Version 2,

Technical Note NCAR/TN-486+STR, 88 pp., National Center for Atmospheric Research, Boulder, CO.

Suzuki, S., Shiokawa, K., Otsuka, Y., Ogawa, T., Nakamura, K., Nakamura, T., 2007. A concentric gravity wave structure in the mesospheric airglow images. J. Geophys. Res. 112, D02102, http://dx.doi.org/10.1029/2005JD006558.

Suzuki, S., Vadas, S.L., Shiokawa, K., Otsuka, Y., Kawamura, S., Murayama, Y., 2013. Typhoon-induced concentric airglow structures in the mesopause region. Geophys. Res. Lett. 40, 5983–5987, http://dx.doi.org/10.1002/2013GL058087.

Taylor, M.J., Haphood, M.A., 1988. Identification of a thunderstorm as a source of short period gravity waves in the upper atmospheric nightglow emissions. Planet Space Sci. 36 (4), 975–985.

Vadas, S., Yue, J., Nakamura, T., 2012. Mesospheric concentric gravity waves generated by multiple convection storms over the North America Great Plain. J. Geophys. Res. Atmosphere 117, D07113, http://dx.doi.org/10.1029/2011JD017025.

Yue, J.S., Vadas, C.-Y., She, T., Nakamura, S., Reising, H., Liu, P., Stamus, D., Krueger, W., Lyons, T. Li, 2009. Concentric gravity waves in the mesosphere generated by deep convective plumes in the lower atmosphere near Fort Collins, Colorado. J. Geophys. Res. 114, D06104, http://dx.doi.org/10.1029/2008JD011244.

Yue, J., Hoffmann, L., Joan Alexander, M., 2013. Simultaneous observations of convective gravity waves from a ground-based airglow imager and the AIRS satellite experiment. J. Geophys. Res. Atmos. 118, 3178–3191, http://dx.doi.org/10.1002/jgrd.50341.

Yue, J., Thurairajah, B., Hoffmann, L., Alexander, M.J., Chandran, A., Taylor, M., Russell III, J.M., Randall, C., Bailey, S.M., 2014. Concentric gravity waves in polar mesospheric clouds from the Cloud Imaging and Particle Size (CIPS) experiment. J. Geophys. Res. Atmos. 119, 5115–5127, http://dx.doi.org/10.1002/2013JD021385.